AFRL-RY-WP-TR-2020-0005

THE UNBOUNDED AND BOUNDED BOUNDARY LAYER MODELS FOR FLOW ALONG A WALL

David Weyburne

Optoelectronics Technology Branch
Aerospace Components & Subsystems Division

FEBRUARY 2020
Final Report

AIR FORCE RESEARCH LABORATORY
SENSORS DIRECTORATE
WRIGHT-PATTERSON AIR FORCE BASE, OH 45433-7320
AIR FORCE MATERIEL COMMAND
UNITED STATES AIR FORCE

NOTICE AND SIGNATURE PAGE

Using Government drawings, specifications, or other data included in this document for any purpose other than Government procurement does not in any way obligate the U.S. Government. The fact that the Government formulated or supplied the drawings, specifications, or other data does not license the holder or any other person or corporation; or convey any rights or permission to manufacture, use, or sell any patented invention that may relate to them.

This report was cleared for public release by the USAF 88th Air Base Wing (88 ABW) Public Affairs Office (PAO) and is available to the general public, including foreign nationals. Copies may be obtained from the Defense Technical Information Center (DTIC) (http://www.dtic.mil).

AFRL-RY-WP-TR-2020-0005 HAS BEEN REVIEWED AND IS APPROVED FOR PUBLICATION IN ACCORDANCE WITH ASSIGNED DISTRIBUTION STATEMENT.

// Signature//	// Signature//
DAVID T. TOMICH, Program Manager Optoelectronics Technology Branch Aerospace Components & Subsystems Division	FRED E. ARNOLD, Branch Chief Optoelectronics Technology Branch Aerospace Components & Subsystems Division

This report is published in the interest of scientific and technical information exchange, and its publication does not constitute the Government's approval or disapproval of its ideas or findings.

*Disseminated copies will show "//Signature//" stamped or typed above the signature blocks.

REPORT DOCUMENTATION PAGE

Form Approved
OMB No. 0704-0188

1. REPORT DATE *(DD-MM-YY)*	2. REPORT TYPE	3. DATES COVERED *(From - To)*
February 2020	Final	01 November 2014 – 13 April 2015

4. TITLE AND SUBTITLE

THE UNBOUNDED AND BOUNDED BOUNDARY LAYER MODELS FOR FLOW ALONG A WALL

5a. CONTRACT NUMBER
In-house

5b. GRANT NUMBER

5c. PROGRAM ELEMENT NUMBER
N/A

6. AUTHOR(S)
David Weyburne

5d. PROJECT NUMBER
N/A

5e. TASK NUMBER
N/A

5f. WORK UNIT NUMBER
N/A

7. PERFORMING ORGANIZATION NAME(S) AND ADDRESS(ES)
Optoelectronics Technology Branch
Aerospace Components & Subsystems Division
Air Force Research Laboratory, Sensors Directorate
Wright-Patterson Air Force Base, OH 45433-7320
Air Force Materiel Command, United States Air Force

8. PERFORMING ORGANIZATION REPORT NUMBER
AFRL-RY-WP-TR-2020-0005

9. SPONSORING/MONITORING AGENCY NAME(S) AND ADDRESS(ES)

Air Force Research Laboratory
Sensors Directorate
Wright-Patterson Air Force Base,
OH 45433-7320
Air Force Materiel Command
United States Air Force

Air Force Office of Scientific Research
Public Affairs (AFOSR)
875 North Randolph Street
Suite 325, Room 3112
Arlington, VA 22203

10. SPONSORING/MONITORING AGENCY ACRONYM(S)
AFRL/RYDH

11. SPONSORING/MONITORING AGENCY REPORT NUMBER(S)
AFRL-RY-WP-TR-2020-0005

12. DISTRIBUTION/AVAILABILITY STATEMENT
Approved for public release; distribution is unlimited.

13. SUPPLEMENTARY NOTES
PAO Case Number 88ABW-2020-0074, Clearance Date 9 January 2020. Report contains color.

14. ABSTRACT
In an earlier report (AFRL-RY-WP-TR-2020-0004) a new unbounded boundary layer model for describing flow along a wall was introduced. In the new model, the flow asymptotes to the free stream value. Herein, we do a more extensive comparison between the bounded and unbounded boundary layers using flow simulations on a large gap channel consisting of two parallel flat plates. The channel plate gap distance is increased until an unbounded condition is reached. For laminar flow conditions, the required gap is found to be over seven meters, far exceeding the typical wind tunnel dimensions. The results also indicate that the often-used validation of wind tunnels using Blasius profiles is misleading.

15. SUBJECT TERMS
boundary layer theory, unbounded boundary layer, Blasius comparison, inertial boundary layer, laminar flow

16. SECURITY CLASSIFICATION OF:			17. LIMITATION OF ABSTRACT:	18. NUMBER OF PAGES	19a. NAME OF RESPONSIBLE PERSON (Monitor)
a. REPORT	b. ABSTRACT	c. THIS PAGE			David Weyburne
Unclassified	Unclassified	Unclassified	SAR	30	19b. TELEPHONE NUMBER *(Include Area Code)* N/A

Table of Contents

Section **Page**

List of Figures ii
1. SUMMARY 1
2. INTRODUCTION 2
3. LARGE GAP 2-D CHANNEL MODEL SIMULATION 6
   3.1 Wide Gap Channel Simulation 6
   3.2 Unbounded Boundary Layer Peak Location 11
   3.3 Simulation for Theoretical Modeling 12
4. DISCUSSION 14
5. CONCLUSION 16
6. REFERENCES 17
APPENDIX A: THE BOUNDARY LAYER THICKNESS 19
APPENDIX B: POTENTIAL FLOW ESTIMATION OF THE INERIAL BOUNDARY LAYER THICKNESS 21
APPENDIX C: THE BLASIUS AND FALKNER-SKAN SCALINGS 23
LIST OF ABBREVIATIONS, ACRONYMS, AND SYMBOLS 25

List of Figures

Figure **Page**

Figure 1: The Incomplete Traditional Boundary Layer Model for Laminar Flow a long a Flat Plate in a Wind Tunnel 2
Figure 2: Schematic Drawing depicting new Boundary Layer Model for Unbounded Flow..... 3
Figure 3: Side view of Simulated Air Flow in a 1 *m* high by 8 *m* long channel with an Inlet u_0 of 0.9375 *m/s* Air Flow at RT 6
Figure 4a: The Centerline *x*-pressure Gradient at various Gap Distances (*H*) 7
Figure 4b: The *x*-pressure Gradient Profile for various Gap Distances (*H*) 7
Figure 5a: The $u(x,y)$ Velocity Profiles at Locations along the Channel for $H = 1$ *m* 8
Figure 5b: The $u(x,y)$ Velocity Profiles at Locations along the Channel for $H = 3$ *m* 8
Figure 5c: The $u(x,y)$ Velocity Profiles at Locations along the Channel for $H = 7$ *m* 8
Figure 5d: The $u(x,y)$ Velocity Profiles at Locations along the Channel for $H = 10$ *m* 8
Figure 6a: The $v(x,y)$ Velocity Profiles at Locations along the Channel for $H = 1$ *m* 9
Figure 6b: The $v(x,y)$ Velocity Profiles at Locations along the Channel for $H = 3$ *m* 9
Figure 6c: The $v(x,y)$ Velocity Profiles at Locations along the Channel for $H = 7$ *m* 9
Figure 6d: The $v(x,y)$ Velocity Profiles at Locations along the Channel for $H = 10$ *m* 9
Figure 7a: The dP/dy Profiles at Locations along the Channel for $H = 1$ *m* 10
Figure 7b: The dP/dy Profiles at Locations along the Channel for $H = 3$ *m* 10
Figure 7c: The dP/dy Profiles at Locations along the Channel for $H = 7$ *m* 10
Figure 7d: The dP/dy Profiles at Locations along the Channel for $H = 10$ *m* 10
Figure 8a: Comparison of the Boundary Layer Thickness for the Viscous Unbounded Case 11
Figure 8b: The Inertial Boundary Layer Thickness δ_{i2} along the Channel in Figure 8a 11
Figure 9a: The Pressure Coefficient along the Wedge at different Wedge Heights 12
Figure 9b: The *y*-pressure Gradient along the Wedge at different Wedge Heights 12
Figure 10a: Velocity Profiles for $u(x,y)$ for Wedge Flow with C_p shown in Figure 9a 13
Figure 10b: Velocity Profiles for $v(x,y)$ for Wedge Flow with C_p shown in Figure 9a 13

1. SUMMARY

The traditional boundary layer model used in describing laminar and turbulent flow along a wall assumes the flow asymptotes to some velocity that, in general, is not the same as the free stream velocity. This is the type of boundary layer usually observed in wind tunnel experiments. The value of the asymptotic velocity can be manipulated by adjusting the tunnel ceiling height, for example. In contrast, for an unbounded boundary layer, the velocity must asymptote to the inlet free stream value. This is the type of boundary layer encountered on airplane wings in free flight. The traditional boundary layer model does not work for the unbounded boundary layer. In an earlier Air Force Tech Report (AFRL-RY-WP-TR-2020-0004), a new boundary layer model for describing flow along a wall in which the flow is unbounded was introduced. The unbounded boundary layer is characterized by two boundary layer thicknesses. The first is similar to the traditional viscous boundary layer thickness, whereas the second is a new thickness we have termed the inertial boundary layer thickness. This inertial boundary layer thickness accounts for the distance required for the velocity overshoot present at the viscous boundary layer edge to decay to the free stream velocity. In the work herein, we conduct a computer simulation study of laminar flow in a wide gap channel mimicking a standard wind tunnel. The channel gap is increased until an unbounded boundary layer state is obtained. We use the comparison of the boundary layer velocity profiles to the Blasius theoretical model as a way to determine when the unbounded state is reached. The inertial boundary layer thickness is found to be about eighty times thicker than the viscous boundary layer thickness. This is in the same range as the results we found for a NACA0012 airplane wing flying at 0.5 *M* even though the velocity overshoot in the present case is only about 1-3% compared to the 15% overshoot for the wing case. The large inertial boundary layer region means that it is not possible to achieve an unbounded boundary layer condition in most wind tunnels. For laminar air flow, it is found that a channel plate gap exceeding seven meters is required to reach an unbounded state which far larger what is available in most wind tunnels. In addition, we explore the relationship of the velocity profiles to the theoretical flow models. The large gap parallel channel results are found to be well represented by the Blasius theoretical model in the near wall region. However, it is also found that the often-used practice of setting up zero pressure gradient flows to mimic the Blasius theoretical flow solution is misleading. What we find is that even though the velocity profiles appear to look Blasius-like, the resulting normal velocity profiles and the normal pressure gradient profiles do not display Blasius type behavior. Furthermore, we find that the standard velocity profile approach is not very sensitive to the pressure gradient in the flow direction and that a wide range of flow states can produce the misleading Blasius type profiles.

2. INTRODUCTION

The boundary layer concept was first developed by Ludwig Prandtl[1] as a means to describe fluid flow along a wall. The traditional interpretation of this concept for 2-D flow is depicted in Fig. 1. It assumes that the velocity in the flow direction starts out as zero velocity at the wall (no-slip) and then gradually asymptotes to a boundary layer edge velocity, $u_e(x)$, as one moves normal to the wall into the fluid. This traditional boundary layer description has worked well for the past 100 years. Asymptotic velocity profiles like those depicted in Fig. 1 are routinely measured in wind tunnels around the world. However, stepping back, this behavior is at odds with expectations in that one should expect the velocity to asymptote to the free stream inlet velocity u_∞, not some boundary layer edge velocity $u_e(x)$. The explanation for this anomalous asymptotic behavior is that the boundary layer must be interacting with another pressure field. We call this interacting condition the "bounded" boundary layer. Based on the observation that most experimental velocity profiles display asymptotic behavior that does **not** return to the free stream value, we can conclude that in most wind tunnels, the bounded condition is what is normally encountered. A further indication of this "bounded" behavior in wind tunnels comes from the fact that this upper-lower boundary layer interaction is routinely used in wind tunnels to construct flows along the plate with either a zero-pressure gradient (ZPG), a favorable pressure gradient (FPG), or an adverse pressure gradient (APG) by adjusting the ceiling height along the flow direction. An important short coming of the traditional bounded boundary layer model depicted in Fig. 1 is that it does not include any indication of the interaction with the pressure field inducing asymptotic behavior and is therefore an incomplete depiction of the flow.

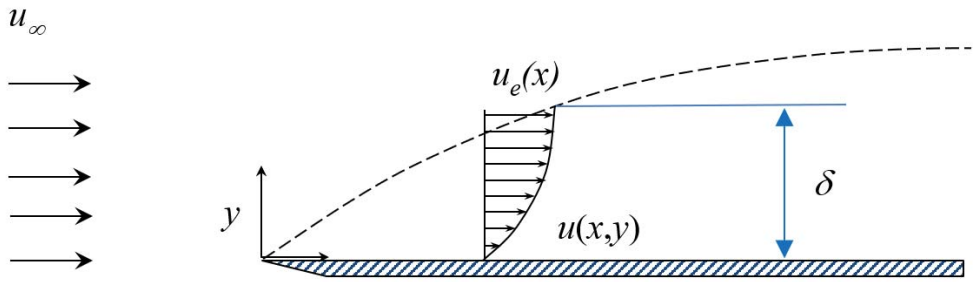

Figure 1: The Incomplete Traditional Boundary Layer Model for Laminar Flow a long a Flat Plate in a Wind Tunnel

The bounded boundary layer description works for most wind tunnel experiments but what model do we use for external flows like those that occur for air flow over a wing in flight? In these flows, the velocity above the wall-wing does **not** asymptote to a boundary layer edge velocity but instead returns to the free stream velocity at some point above the wall-wing. Hence, the traditional boundary layer model does not work for this case. In an earlier report,[2] we introduced a new boundary layer model that we refer to as the "unbounded boundary layer" model. In this model, the velocity above the plate peaks and then slowly returns to the free stream inlet flow velocity u_∞. This model is depicted in Fig. 2. As a means of handling the theoretical aspects of the model, two regions are identified; the first encompasses what was the traditional viscous boundary layer and a second region above the viscous boundary layer region that we call the inertial boundary layer region since viscous forces are mostly absent. The

boundary layer thickness next to the plate-airfoil is given by $\delta_{\max}$ or, equivalently, δ_v. This region is characterized by the presence of viscous effects. The value of $\delta_{\max}$ is just the *y*-value where the velocity profile $u(x, y)$ peaks. This value appears to be well correlated with the viscous boundary layer thickness[3,4] given by δ_v, at least for the one laminar flow dataset we studied on an airfoil.[5] Above this viscous region, the inertial boundary layer region starts at the velocity profile peak and gradually changes to the free steam velocity u_∞. In the earlier report, we used the central moment method[3,4] to characterize the thickness and shape of this region (a short summary of the relevant equations is given in Appendix A). The thickness δ_i is the distance required for the velocity overshoot to return to the free stream velocity.

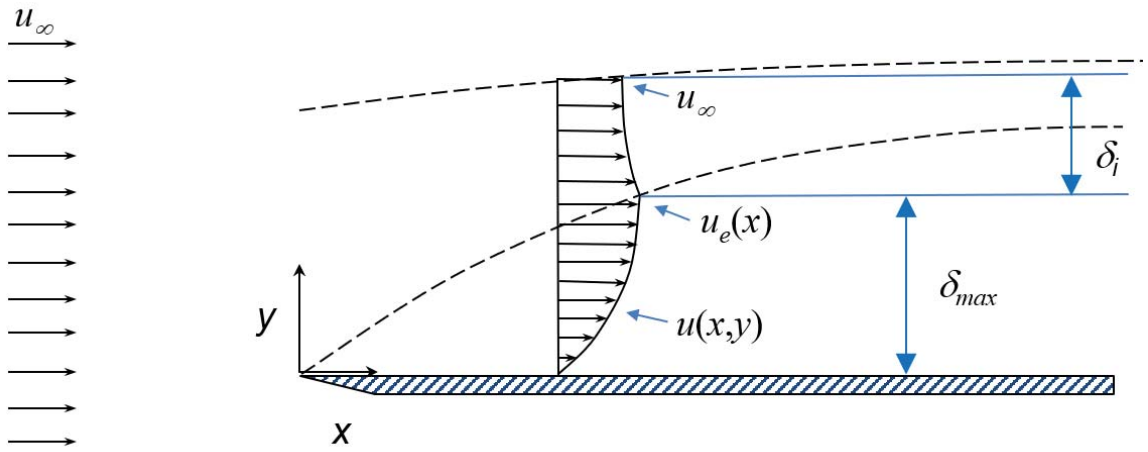

Figure 2: Schematic Drawing depicting new Boundary Layer Model for Unbounded Flow
Drawing is not to scale since, in general, $\delta_i >> \delta_{\max}$.

What is NOT addressed in Fig. 2 is the case for turbulent boundary layer flow on an airfoil. It is straightforward to add the turbulent boundary layer to the model shown in Fig. 2, but for simplicity, we will ignore the presence of a turbulent region for now.

In one context, the inertial boundary layer has been addressed before. For flow simulation calculations, it is necessary to choose the outer simulation extents for external flows. One naturally wants to choose values that insure that the plate-wing influences on the flow in the outer region are no longer significant and that the outer flow behaves essentially as the free stream. In this context, the boundary layer extents are equivalent to the inertial boundary layer thickness. Hirsch[6] studied the computational fluid dynamics (CFD) simulations of exterior flows and determined that the boundary layer extents in both the flow and normal to the flow directions should be about 50 cords. Vaughn[7] did a CFD study of laminar flow over a flat plate and concluded that 20 plate lengths is adequate. More recently, Nigam[8] used a simple potential flow argument to show that 100 obstacle lengths (here interrupted as the viscous boundary layer) should sufficiently diminish the obstacle influences on the flow in the outer region (the potential flow argument is reproduced with permission in Appendix A).

What is missing from these boundary layer extent approaches is a quantitative measure that can be applied in any context. In the earlier report, Weyburne[2] introduced a central moment method to define the inertial boundary layer thickness and shape. The resulting thickness and shape parameters are all integral quantities of the velocity profile (see Appendix A for a brief overview of the relevant equations). The new boundary layer formulation was applied to a CFD simulation[5] of a NACA0012 wing in order to do a preliminary study of this inertial boundary layer region. It was found that the thickness ratio of the inertial region δ_i to the viscous region δ_v for laminar flow on the wing is over 200 for this 0.5 *M* flow case (based on 4 sigma thicknesses). However, a single simulation result does not allow one to generalize the result for any flow situation. Herein, we undertake a new simulation investigation that begins with the flow situation typical in most wind tunnels. To this end we employ a simple 2-D computer simulation modeling laminar flow in an upper-lower flat plate channel. One of the intents of this effort is to try to answer the question as to what kind of gap is required to go from the bounded to unbounded boundary layer in this wind tunnel mimicking configuration. Starting with typical wind tunnel dimensions (one-meter channel gap), we show that the channel gap must be increased to an astonishing 20 meters to reach the unbounded boundary layer case for laminar air flow at room temperature (RT)! These results are similar to the laminar flow flat plate study of Vaughn[7] if we interrupt the boundary layer extent as δ_i.

The 20-meter gap figure is based on the point where the measured four-sigma δ_i value becomes less than the channel half-height. (The four sigma denotes the thickness given by the mean location plus four times the sigma value). However, while the four-sigma value is conceptually valid, there is nothing special about four-sigma as compared to two or three sigma thicknesses, for example. Two, three, and four sigma-based thickness values have all been used at various times in different scientific applications. In order to try to put some physics into the choice of which sigma value to use, a second, more relevant, criterion is also examined. The idea is to find the gap separation distance where the scaled profiles in the boundary layer no longer show signs of interactions with other pressure fields. To investigate this aspect, we simulated 2-D channel flow for various gap separations. The scaled velocity and pressure gradient profiles normal to the wall are then plotted at seven positions along the channel for each gap using the Blasius scaling parameters. What we are searching for is the point where the profiles behave similarly when plotted with the Blasius[9] scaling parameters in the near wall region. Vaughn[7] used this same criterion to determine the boundary layer extent for his simulation study. As it happens, the scaled velocity profiles in the "unbounded" state appear to be well approximated by the Blasius flow solution but not in the bounded state. In what follows, we show that although the $u(x,y)$ profiles show only small changes between the bounded and unbounded states, the normal velocity $v(x,y)$ profiles and the y-pressure gradient profiles show much more profound changes as one goes from a bounded to and unbounded state. Although there is no sharp boundary, it appears as though for laminar flow on a flat plate, this criterion would indicate the bounded to unbounded transition occurs when the half channel height is $(H/2) \cong 80\,\delta_v$. For the results herein, the **two-sigma** thickness based value of δ_i (mean plus two sigma) appears to be the best choice to track this boundary criterion. In order to denote this, we will use δ_{i2} to represent the mean plus two times sigma for the inertial boundary layer region. For the laminar flow case studied herein, this would mean a wind tunnel 7-10 meters high would be necessary to reach an

unbounded state which is significantly higher than what is available in most wind tunnels used to date.

A second set of experiments is performed to study the flow that develops in a typical channel flow mimicking a standard one-meter high wind tunnel. We find that the simulated flow that develops in a flat wall channel in a wind tunnel does not produce Blasius[9] or Falkner-Skan[10] type flows. This is also what is apparently observed in most wind tunnel experiments. The implication of a non-similar flow is that one must carefully map out the velocities and pressure gradients over the whole plate if one wants to use this configuration for an experiment that can be reproduced in another facility. This would be difficult since the normal velocity profiles and/or normal pressure gradient profiles are rarely if ever measured. Alternatively, one can try to set the flow up into a known condition. For example, it is fairly routine in wind tunnel-based experimental efforts to try to reproduce the Blasius flow condition by forcing the pressure gradient in the flow direction to be zero. In this scenario, one might think that one has a good map of the velocity and pressure fields.

To test this scenario we set up a series of experiments to try to verify the existence of forced Blasius[9] or Falkner-Skan[10] type flows in a wind tunnel sized channel. In the first set of experiments, we tried to produce Blasius type flow by simply tilting the plates in the channel to induce a zero-pressure gradient. We show that the small angle wedge flow is **not** well represented by the Blasius or Falkner-Skan theoretical models. The $u(x,y)$ velocity profiles behave similarly when scaled with the Blasius scaling parameters but the normal velocity profiles and the normal pressure gradient profiles do not show similarity for the Blasius or Falkner-Skan scalings. To try to correct this situation, we tried replacing the top flat plate with a tilted and/or curved plate. This is a fairly standard way (see, for example, Jovanović, et. al.[11] and Harun, et. al.[12]) to try to force the flow to take on a FPG, APG, or a ZPG pressure gradient in the flow direction. While effective in forcing a zero pressure gradient and Blasius-like $u(x,y)$ velocity profiles, the Blasius or Falkner-Skan scaling parameters did **not** show similar behavior for the normal velocity profiles or the normal pressure gradient profiles no matter what we tried.

In what follows, we first start by looking at the gap requirement to reach an unbounded flow condition. We then follow up with an experiment to look at the correlation between the viscous boundary thickness and the velocity profile maximum value. Finally, we look at the problem of trying to induce unbounded boundary layer behavior in a standard will tunnel configuration.

3. LARGE GAP 2-D CHANNEL MODEL SIMULATION

Our first objective is to study the transition from bounded to unbounded boundary layers. There are a number of simulation geometries we could have used but as a start, we went with a large gap 2-D flat plate channel geometry. The advantage of this geometry is that once an unbounded state is achieved, the geometry mimics the flat plate flow depicted in Fig. 2. To keep the interpretation as simple as possible, it was decided to initially consider just laminar flow. To insure turbulent effects are not present, the length of the channel and the air inlet velocity are adjusted so that the conditions at the channel exit corresponds to the critical Reynolds number for laminar-turbulent transition ($Re_x = 5x10^5$). As a start, a one meter high by eight-meter long channel geometry is used with a short half meter inlet section included so that the effects of the channel inlet edges can be accurately simulated. A side view of the initial simulation geometry is depicted in Fig. 3. OpenFoam simulation software is used with multi-grade meshing in both the flow direction and normal to the wall directions. The SimpleFoam solver is used, incompressibility assumed, and the exit set to a zero-pressure boundary condition. Mesh sizes ranged from 1800 x 750 for the one-meter gap to 2200 x 1150 for the larger gap simulations. In general, the simulations are run until the velocity and pressure residuals dropped below $1x10^{-6}$.

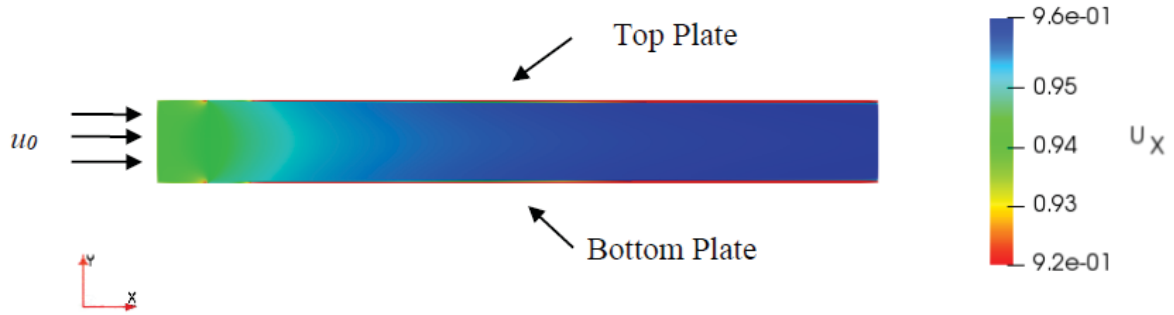

Figure 3: Side view of Simulated Air Flow in a 1 *m* high by 8 *m* long channel with an Inlet u_0 of 0.9375 *m/s* Air Flow at RT

3.1 Wide Gap Channel Simulation

The first set of simulations consisted of RT airflow in an 8-meter long flat plate channel. The inlet velocity is set at 0.9375 *m/s* resulting in a Re_x of $5x10^5$ at the channel exit. The gap distance value is initially one meter with subsequent simulations having larger gaps. Slices in both the flow direction and the normal to the wall direction are taken and used to capture profile flow information. The difference between the bounded and unbounded states is that for the bounded state, there must be some external pressure field interacting with the boundary layers pressure field. It is therefore important to understand all of the pressure fields present in the channel. To that end, consider the *x*-pressure gradient profile plots in Fig. 4. The centerline *x*-pressure gradient plot (Fig. 4a) is a good indication of how the various *y*-profile plots are going to behave. A key assumption of the Blasius theoretical model is that the pressure gradient in the flow direction must be constant. Looking at Fig. 4a, the pressure gradient is only constant for the largest channel gap. It is decidedly not constant at the 1-meter gap typically used in real wind tunnels. This pressure gradient effect should therefore be reflected in the scaled plots for the *x* and *y* velocity profiles as well as the *y*-pressure gradient profiles.

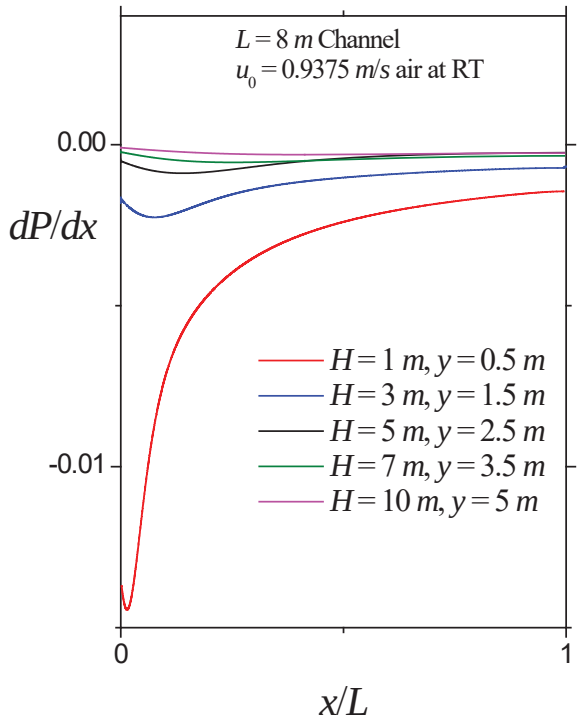

Figure 4a: The Centerline *x*-pressure Gradient at various Gap Distances (*H*)

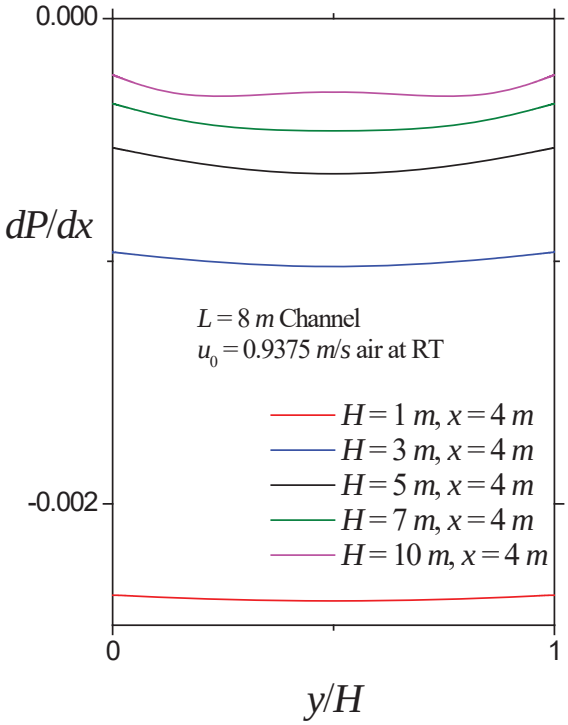

Figure 4b: The *x*-pressure Gradient Profile for various Gap Distances (*H*)

It should also be the case that the *x*-pressure gradient should be constant in the direction normal to the wall (Fig. 4b). The interesting aspect here is that it appears that the *x*-pressure gradient is not constant in the near wall regions for the largest gap. The consequences of this will be taken up in the Discussion section.

The results of Fig.4a should be reflected in the behavior of the profiles as one moves along the channel. In Figs, 5-7 (on pages 8-10), the $u(x,y)$ profiles, the normal $v(x,y)$ profiles, and the normal *y*-pressure gradient profiles are plotted at seven locations along the channel plate in the flow direction for four channel gap values. Various scaling origins were tried and in the end scaling with the x=0 location seemed to work best (see Appendix C for the scaling details). The results in Fig. 5 (page 8) indicate that the $u(x,y)$ velocity profiles are not very sensitive to the channel gap. Just looking at Fig. 5, one could easily conclude that all but the one-meter gap profiles display similar behavior using the Blasius scaling. It is not until one looks at the normal velocity profiles or the *y*-pressure gradient profiles that one begins to see significant differences. Fig. 6 and Fig. 7 (pages 9 and 10) together indicate the likely bounded to unbounded boundary layer transition occurs when the gap distance is in the 7-10 meter range. (It is also apparent that the profiles at x = 7 *m* shows that some flow disruption exists in the exit region).

It is also worth emphasizing that this good comparison between the Blasius result and the simulation result for the unbounded boundary layer (Fig. 6d) is only true in the near wall region. The good agreement between the Blasius normal velocity and the simulation results rapidly degrades as the distance from the wall increases. The simulation result decline until it reaches zero at the gaps midpoint which is obviously not in line with the Blasius prediction.

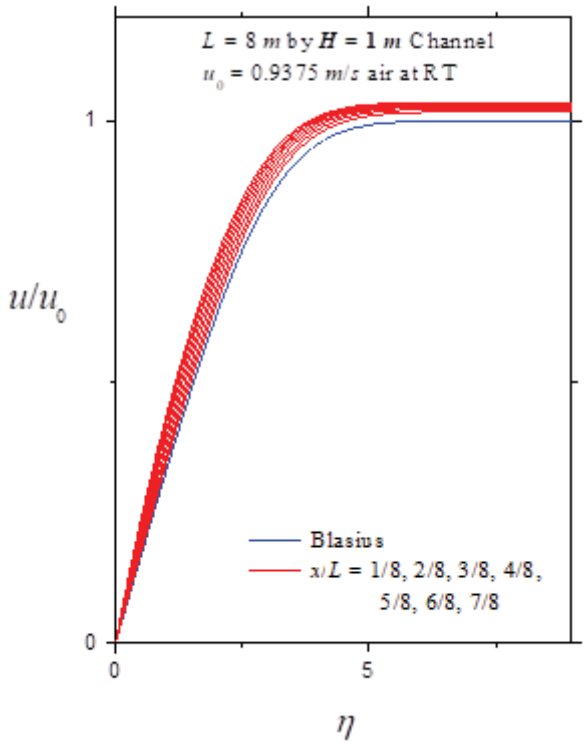

Figure 5a: The *u*(*x*,*y*) Velocity Profiles at Locations along the Channel for *H* = 1 *m*

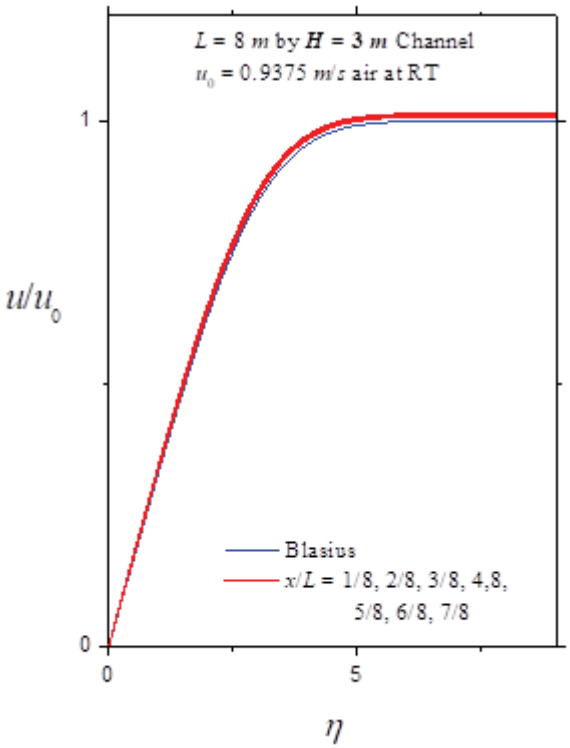

Figure 5b: The *u*(*x*,*y*) Velocity Profiles at Locations along the Channel for *H* = 3 *m*

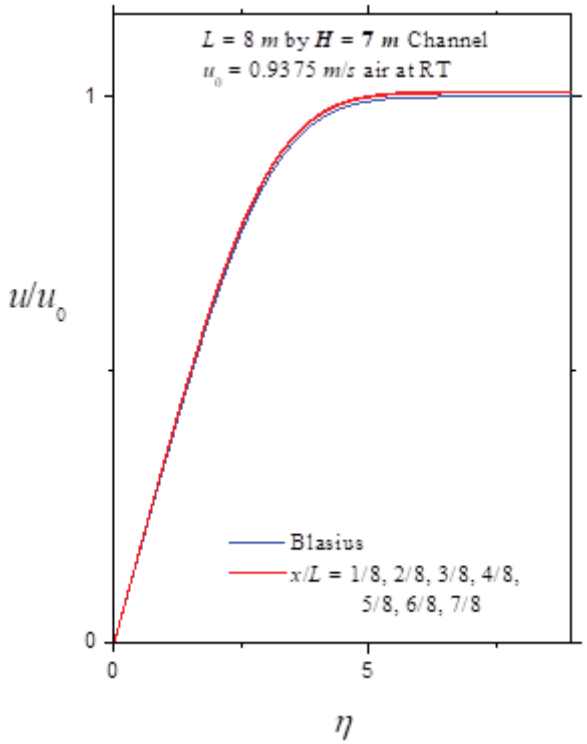

Figure 5c: The *u*(*x*,*y*) Velocity Profiles at Locations along the Channel for *H* = 7 *m*

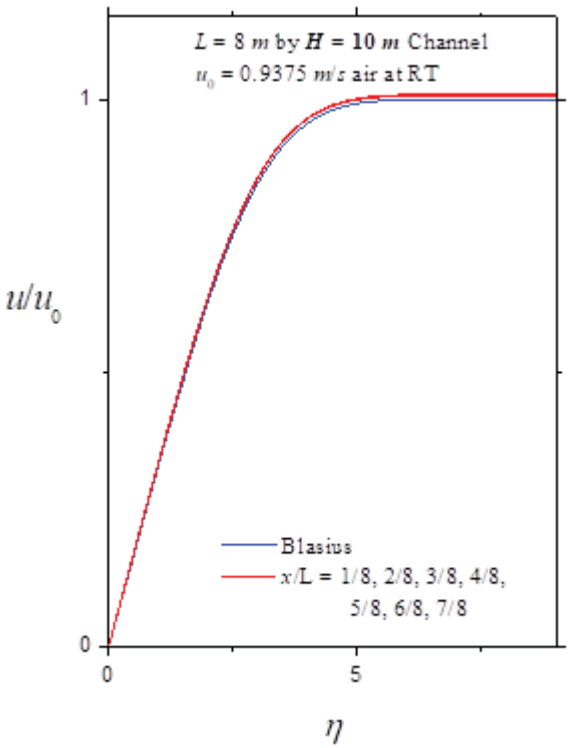

Figure 5d: The *u*(*x*,*y*) Velocity Profiles at Locations along the Channel for *H* = 10 *m*

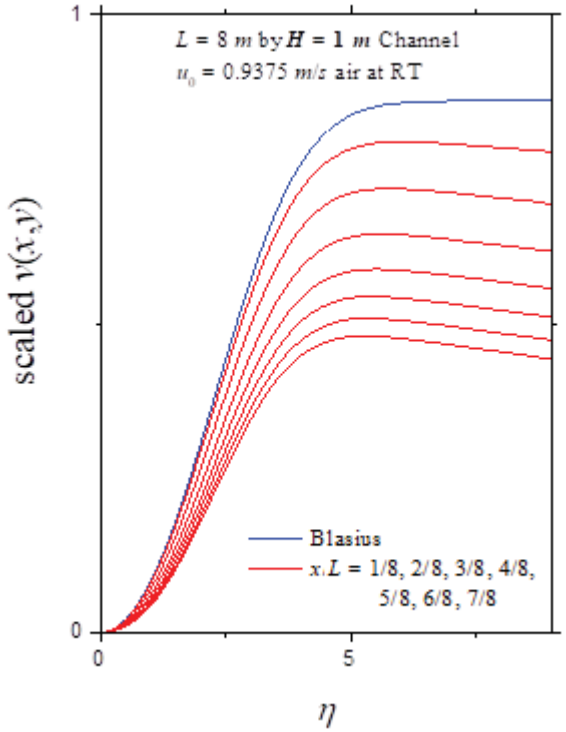

Figure 6a: The *v*(*x*,*y*) Velocity Profiles at Locations along the Channel for *H* = 1 *m*

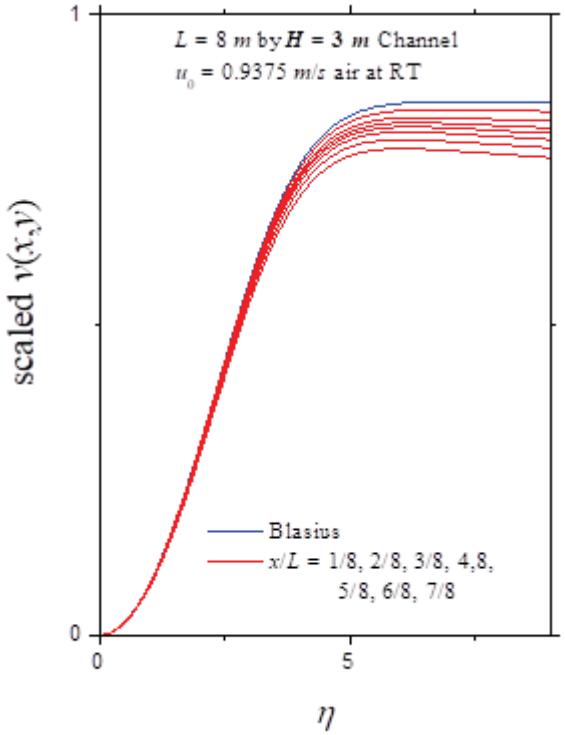

Figure 6b: The *v*(*x*,*y*) Velocity Profiles at Locations along the Channel for *H* = 3 *m*

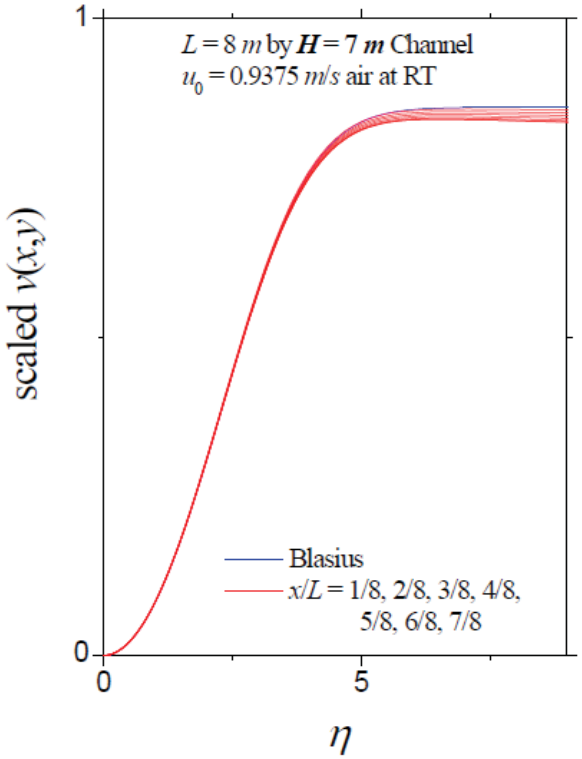

Figure 6c: The *v*(*x*,*y*) Velocity Profiles at Locations along the Channel for *H* = 7 *m*

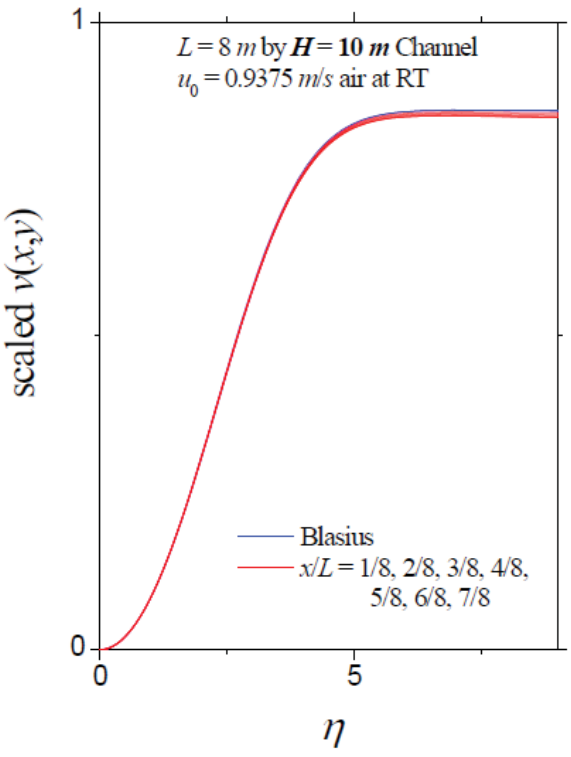

Figure 6d: The *v*(*x*,*y*) Velocity Profiles at Locations along the Channel for *H* = 10 *m*

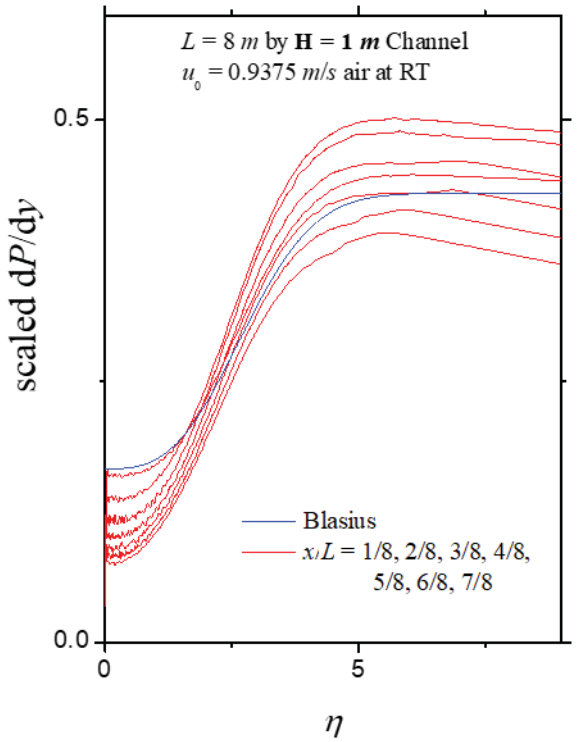

Figure 7a: The d*P*/d*y* Profiles at Locations along the Channel for *H* = 1 *m*

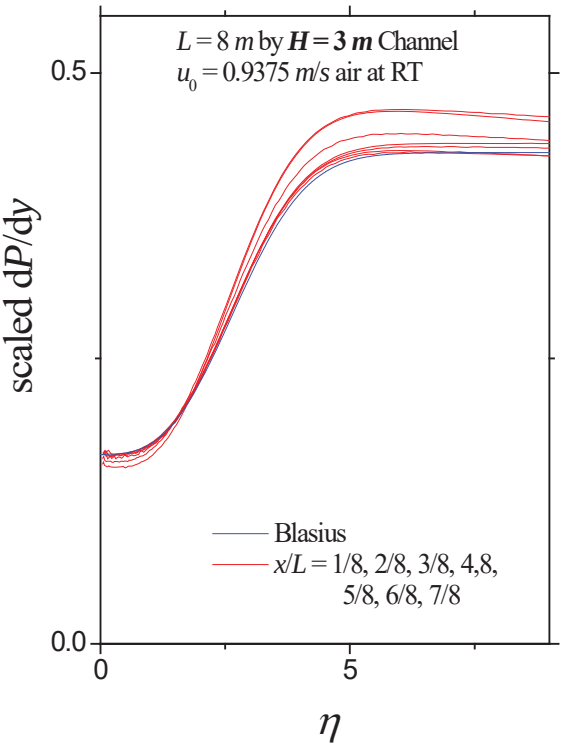

Figure 7b: The d*P*/d*y* Profiles at Locations along the Channel for *H* = 3 *m*

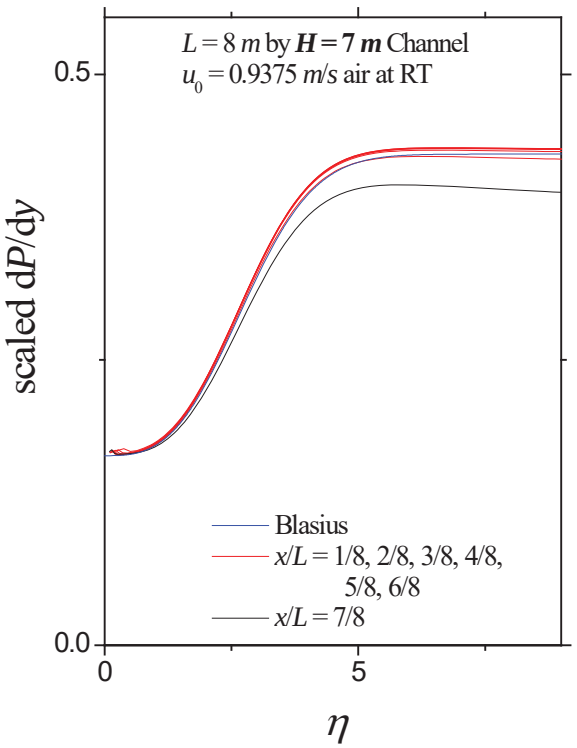

Figure 7c: The d*P*/d*y* Profiles at Locations along the Channel for *H* = 7 *m*

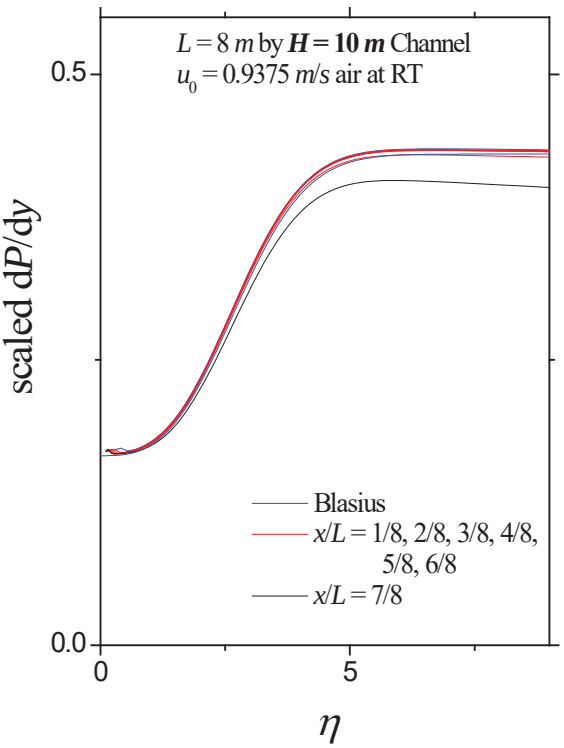

Figure 7d: The d*P*/d*y* Profiles at Locations along the Channel for *H* = 10 *m*

3.2 Unbounded Boundary Layer Peak Location

One aspect of the unbounded boundary layer model depicted in Fig. 2 is that we use the peak velocity located at δ_{max} as the boundary between the viscous and inertial regions. The use of the peak velocity location is mostly for convenience; it is easily measured and conceptualized. In the earlier report on the NACA0012 wing, it was demonstrated that there was a very good correlation between δ_{max} and $\delta_v^{2.6}$ where $\delta_v^{2.6}$ is the viscous boundary layer thickness given by viscous mean location, ω, plus 2.6 times the viscous sigma value σ_v (see Appendix A). In Fig. 8, we show the correlation for one of the unbounded laminar flow cases herein. While the difference between the 2.6 and 4.3 sigma may seem like a lot, for the case herein it is the difference between the δ_v value is 0.064 *m* versus 0.047 *m* for the profiles taken at the four-meter channel location. This difference may be correlated with the velocity overshoot. More work needs to be done to understand the exact nature of the relationship between the viscous thickness and the maximum velocity location but results thus far indicate that there is a strong correlation between the two parameters. In Fig. 8b we show the inertial boundary layer thickness for this same flow situation. By inspection, one can observe that the inertial boundary layer thickness is on the order of 60-80 times as thick as the viscous boundary layer thickness.

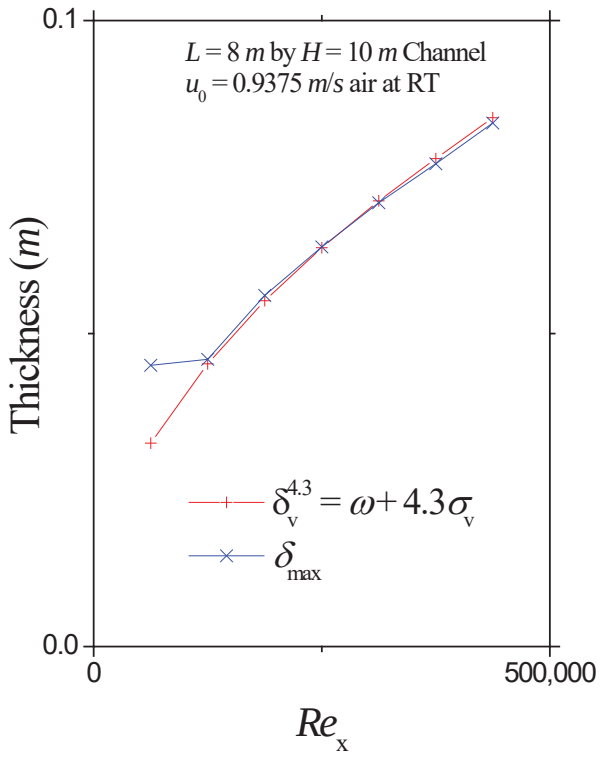

Figure 8a: Comparison of the Boundary Layer Thickness for the Viscous Unbounded Case

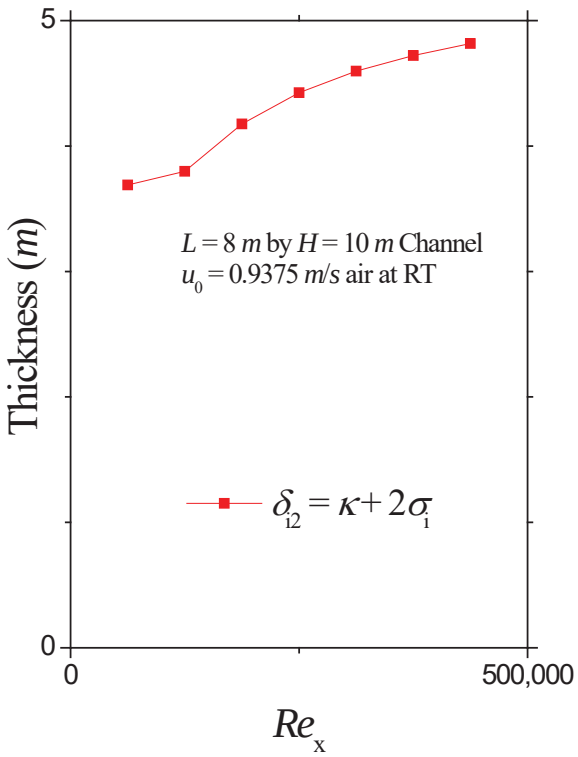

Figure 8b: The Inertial Boundary Layer Thickness δ_{i2} along the Channel in Figure 8a

3.3 Simulation for Theoretical Modeling

The next question we sought to answer is whether there is way to mimic the unbounded boundary layer in a standard wind tunnel. For these experiments, the simulated wind tunnel dimensions are kept at one meter high by eight-meter long channel with a one-half meter inlet section. For our first effort in this area, we tried to obtain a zero-pressure gradient by simply tilting the plates. This type of tilting has been used in the past to try to set the wind tunnel up with a zero-pressure gradient for certain types of experiments (see, for example, J. Jovanović, et al.[11]). The process of establishing a zero-pressure gradient in the wind tunnel is straightforward; simply measure the pressure along the plate and adjust the tilt as necessary. For the flow simulations, the process is similar; try different tilts until the pressure coefficient is as close to zero as possible. Fig. 9 shows the centerline (y=0.5 m) pressure coefficient and centerline pressure gradient as a function of distance along the channel/wedge for different tilts. The use of the wedge succeeded in reducing the pressure coefficient along much of the wedge's length. For the wedge with the H=1.0026 m exit, the average pressure coefficient is C_p=-0.002 with a standard deviation of 9e-4 m over x/L = 0.2 to x/L=1. In spite of the very small pressure coefficient over most of the channel/wedge for this case, we can see the pressure gradient is still not constant (Fig. 9b). This is reflected in the resulting $u(x,y)$ and $v(x,y)$ profiles shown in Fig. 10. A range of m-values for the Falkner-Skan velocity power coefficient (Appendix C) were tested to try to collapse the profiles. None were completely successful. The m=0 value worked for the $u(x,y)$ profiles but we were unable to induce any collapse for the $v(x,y)$ profiles.

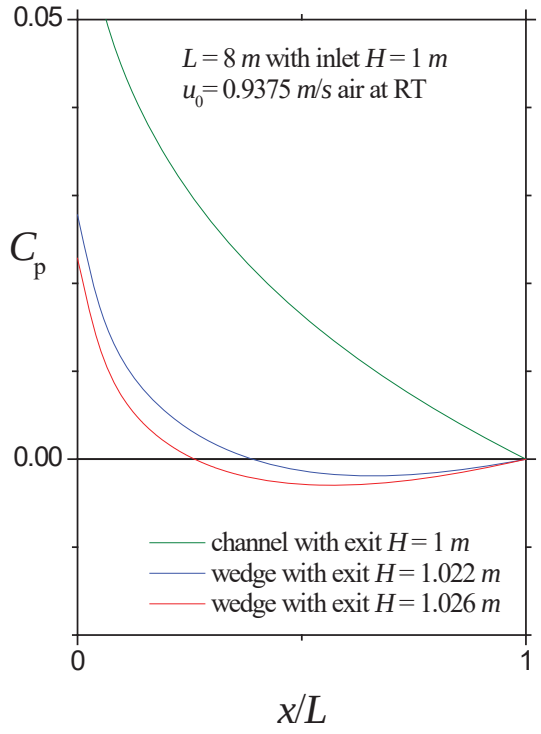

Figure 9a: The Pressure Coefficient along the Wedge at different Wedge Heights

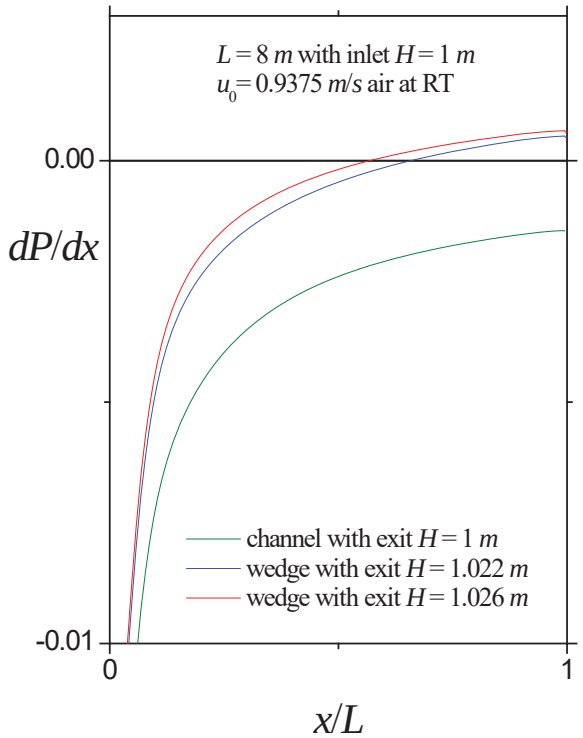

Figure 9b: The y-pressure Gradient along the Wedge at different Wedge Heights

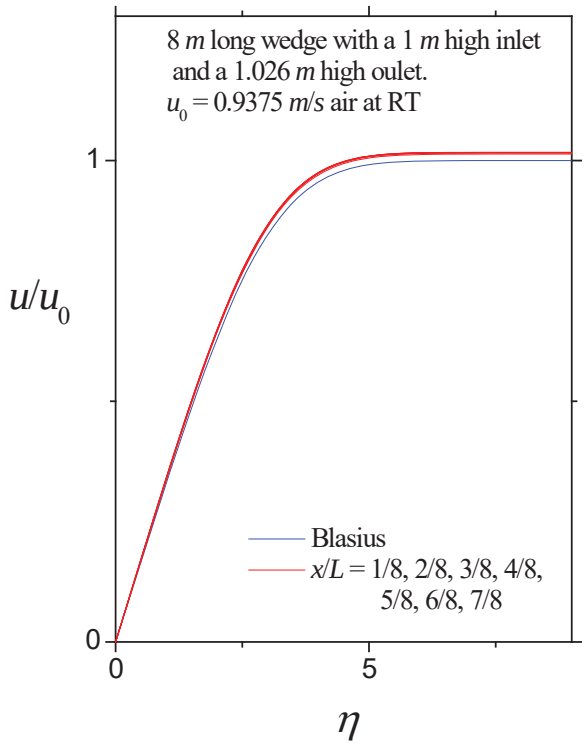

Figure 10a: Velocity Profiles for $u(x,y)$ for Wedge Flow with C_p shown in Figure 9a

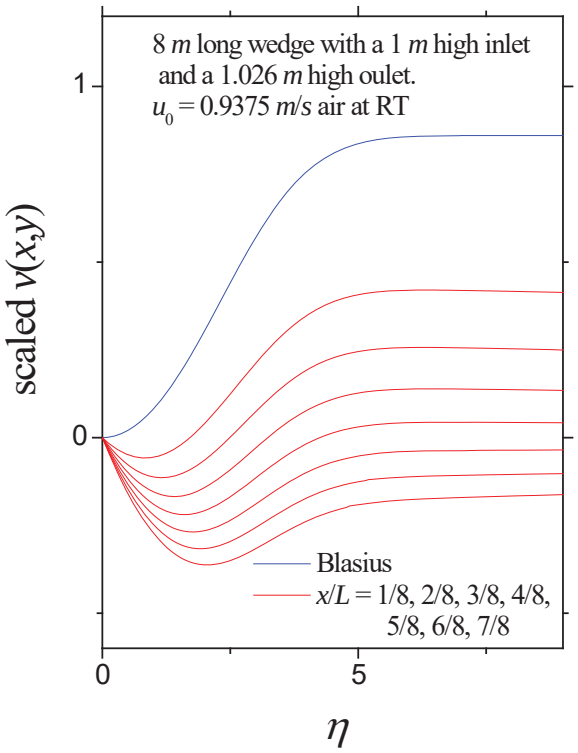

Figure 10b: Velocity Profiles for $v(x,y)$ for Wedge Flow with C_p shown in Figure 9a

In a second set of tests, we tried various tilts, curved top plates, and curve and tilted top plates to achieve Blasius or Falkner-Skan type flow profiles. Even though we are able to obtain average C_p values as low as C_p =-5E-4 over x/L = 0.2 to x/L=1, none of the resulting cases showed true Blasius or Falkner-Skan type flow. The characteristic that sets the unbounded flow case apart is not the low-pressure coefficient value but the flatness of the x-pressure gradient. The unbounded flow shown in Fig. 4 (H = 10 m, L = 8 m) had an average pressure coefficient value of C_p = 0.003 and an average x-pressure gradient value of dP/dx = -5e-4 with a standard deviation of 5e-5. For the tilted-curved top plate case that had the C_p =-5e-4 value, the x-pressure gradient value is dP/dx =7e-4 with a standard deviation of 1.5e-3. The standard deviation results indicate that it is not low value of the pressure coefficient or the absolute value of the pressure gradient that is important but instead it appears the important factor is the flatness of the gradient of the pressure coefficient in the flow direction. Not unexpectedly, the results indicate that the x-pressure gradient over the channel length must be constant to generate Blasius or Falkner-Skan type flow profiles just as the theory dictates.

4. DISCUSSION

The traditional boundary layer model assumes that the velocity profile at a position x along the wall asymptotes to $u_e(x)$, a constant value. The universal acceptance of this model appears to be partly driven by the fact that it is believed that the theoretical approaches of Blasius[9] and Falkner-Skan[10] closely describe this flow situation and partly by the fact that wind tunnel measurements seem to confirm their existence. Most wind tunnel experiments do show something close to asymptotic behavior in the velocity profiles tail region, at least in the near wall region. In fact, even our unbounded laminar flow simulation case studied herein had behavior close to a constant tail region (velocity overshoot ~1%). If one replaces the velocity scaling u_∞ by $u_{\max}$ in Fig. 5d, for example, the experimental curves appear to overlap with the Blasius curve completely. In a wind tunnel, the presence of experimental noise and the very slow relaxation in the inertial boundary layer region would make it easy to completely dismiss the presence of an overshoot of this magnitude. However, no matter how small the velocity overshoot, simple physics dictates that the traditional model depicted in Fig. 1 is at best an approximation of what one would expect to be for an unbounded flow situation. Where the new unbounded model becomes indispensable, is for the case of airfoils or tilted plates. For the laminar flow results herein, the velocity overshoot is about 1% compared to the 15% for the NACA0012 airplane wing[2] flying at 0.5 M case. For the NACA0012 airplane wing case or, presumably, for any tilted plate case with a substantial velocity overshoot, the traditional boundary layer case is just **not** a good representation of the actual flow.

The simulation results herein indicate that the near wall region of unbounded laminar flow along a wall is well represented by the Blasius theoretical model if one ignores the small velocity overshoot. The presence of the velocity overshoot is in direct conflict to the Blasius and Falkner-Skan theoretical models which incorporate a zero-velocity overshoot for the $u(x,y)$ profile. We would argue that the presence of the overshoot is part of the same pressure driven manifestation that results in the generation of the normal velocity in the boundary layer region. One cannot have a unidirectional pressure phenomenon. The pressure forces creating the normal velocity also have to contribute to the near wall $u(x,y)$ profile in the form of a non-constant dP/dx contribution. The simulation results herein (Fig. 4b, H=10 m) confirm that dP/dx is not constant in the boundary layer region for the unbounded boundary layer case (Figs. 5d-7d). We believe this nonconstant dP/dx contribution results in the observed velocity overshoot in the $u(x,y)$ profile. Furthermore, we would argue that this lack of velocity overshoot in the Blasius formulation explains the normal velocity problem encountered in the Blasius theoretical model. The Blasius normal velocity asymptotes to a constant non-zero value which is clearly non-physical. This non-physical aspect of the Blasius formulation (see Lewins[13] and Pantokratoras[14]) has never been satisfactorily addressed and is almost universally ignored in the literature. It is possible that the finite thickness of the inertial boundary layer provides a mechanism to insure the normal velocity profile returns to zero in the free stream.

The other aspect of wind tunnel operation we attempted to elucidate is the practice of setting up zero pressure gradient conditions that mimic the Blasius theoretical model. The misleading aspect of this practice is the expectation that one is setting up a wind tunnel set of conditions in which the flow is “known” over the whole plate/wing where the ZPG condition exists. What we found herein is that in spite of being able to set up near-zero pressure conditions which are much

closer to zero pressure than what can be produced in a wind tunnel setting,[12,16] we were never able to fully reproduce Blasius or Falkner-Skan type profiles. The $u(x,y)$ profiles showed similar Blasius-type behavior but the $v(x,y)$ profiles and y-pressure gradients profiles did not. The bigger question is whether this result is relevant for certain experiments involving stability or laminar-turbulent transition. The answer is not clear. On the one hand, the normal velocity is about one thousand times smaller than the flow velocity along the wall. Since the energy goes as the velocity squared, the energy contained in the normal velocity direction is very small compared to the main flow. However, for cases involving flow stability of one kind or another, small disturbances matter. One can speculate that small disturbances would respond differently depending on the normal velocity and the y-pressure gradient condition on the plate. Hence, stability would also be affected. This may be something simulation studies could elucidate.

In any case, there does not seem to be any recourse for wind tunnel experiments. One can only set up known conditions for the $u(x,y)$ profiles since the $v(x,y)$ and y-pressure gradients are difficult to measure and rarely attempted. The complicating factor in that process is that Blasius-like $u(x,y)$ profiles seem to be fairly easy to produce even for cases where the x-pressure gradient is only marginally close to being constant.

One of the original motivations behind the development off the unbounded boundary layer model was the possibility of developing a complete theoretical approach to airfoil lift. Combining the work we did on the Falkner-Skan y-pressure gradient,[15] with the likelihood that the inertial boundary layer had similarity solutions,[2] we felt that it might be possible to combine these efforts and use a panel-type approach of Drela and Giles[17] to make a completely theoretical approach to lift. The idea would be to divide the wing into panels whose boundaries and velocity profile shape would be dictated by a global energy minimization in both the flow, and normal to the flow, directions. The flow solution in the inertial boundary layer region would be handled by a similarity solution rather than the numerical solution approach used by Drela and Giles.[17] The global energy minimization would be applied to both the x and y directions. Unfortunately, the results herein and earlier[2] indicate that the behavior of the normal velocity and y-pressure gradient in viscous region will have to be neglected since they are not well approximated theoretically (Drela and Giles also neglect the normal velocity and y-pressure gradient effects). The mitigating aspect of this is that the energy content of the normal velocity is very small compared to the main velocity flow and therefore may not significantly affect the result. For example, for the NACA0012 wing at x/c=0.3, the normal velocity profile is less than 2% of the main $u(x,y)$ profile flow.[2] Since the energy goes as the velocity squared, the normal velocity will have only marginal effect on the overall energy minimization process.

5. CONCLUSION

A simple computer simulation study of air flow through a large gap 2-D channel is undertaken in order to help understand the behavior of the bounded and unbounded boundary layers. To reach the unbounded flow condition, the channel height needs to be over seven meters for room temperature airflow, far exceeding the typical wind tunnel dimensions. The large gap channel unbounded flow case is found to be well approximated by the Blasius theoretical model in the near wall region. Additionally, the results also indicate that the often-used validation of wind tunnels using zero-pressure gradient condition is misleading in that it is not possible to fully reproduce Blasius-type flows in a typical wind tunnel.

Acknowledgment

The author acknowledges the support of the Air Force Research Laboratory and Gernot Pomrenke at Air Force Office of Scientific Research.

6. REFERENCES

[1]L. Prandtl, "Über Flüssigkeitsbewegung bei sehr kleiner Reibung," Verhandlungen des Dritten Internationalen Mathematiker-Kongresses in Heidelberg 1904.

[2]D. Weyburne, "A Boundary Layer Model for Unbounded Flow Along a Wall," Air Force Tech report AFRL-RY-WP-TR-2020-0004, https://discover.dtic.mil/, 2020.

[3]D. Weyburne, "A mathematical description of the fluid boundary layer, "Applied Mathematics and Computation," **175**, 1675 (2006). Also D. Weyburne, Erratum, Applied Mathematics and Computation, **197**, 466 (2008).

[4]D. Weyburne, "New thickness and shape parameters for the boundary layer velocity profile," Experimental Thermal and Fluid Science, **54**, 22(2014).

[5]R. Swanson and S. Langer, "Comparison of NACA 0012 Laminar Flow Solutions: Structured and Unstructured Grid Methods," NASA/TM-2016-219003.

[6]C. Hirsch, "Numerical Computation of Internal and External Flows," Volume 2, Computational Methods for Inviscid and Viscous Flows, John Wiley and Sons, New York, 1984, page 385.

[7]M. Vaughn, "Guidelines for Gridding Simple Flows- The Flat Plate in Laminar Flow," Army Tech. Report TR-AMR-SS-08-09, A476652, https://discover.dtic.mil/, 2009.

[8]M. Nigam, "How to Place Inlet and Outlet Boundary Conditions in CFD Simulations," COMSOL Blog, August 20, 2018 (reproduced in Appendix A).

[9]H. Blasius, "Grenzschichten in Flüssigkeiten mit kleiner Reibung," Zeitschrift für Mathematik und Physik, **56**, 1(1908).

[10]V. Falkner and S. Skan, Aero. Res. Coun. Rep. and Mem. no 1314, 1930.

[11]J. Jovanović, B. Frohnapfel, E. Škaljić, and M. Jovanović, "Persistence of the Laminar Regime in a Flat Plate Boundary Layer at very High Reynolds Number," Thermal Science, **10**, 63(2006).

[12]Z. Harun, J. Monty, R. Mathis, and I. Marusic, "Pressure gradient effects on the large-scale structure of turbulent boundary layers," J. Fluid Mech., **715**, J. Fluid Mech., 477(2013).

[13]J. Lewins, "Beyond the boundary layer: the Blasius paradox," Int. J. Mech. Engr. Educ., **27**, 55(1999).

[14]A. Pantokratoras, "Is the ambient transverse velocity in a boundary layer flow non-zero or zero?" arXiv:1002.1787 [physics.flu-dyn], 2010.

[15]D. Weyburne, “The normal to the wall pressure gradients for Blasius and Falkner-Skan boundary layer flow,” Air Force Tech report AFRL-RY-WP-TR-2018-0153, https://discover.dtic.mil/, 2018.

[16]J. Klewicki, W. Saric, I. Marusic, J. Eaton, “Wall-Bounded Flows”, Chapter 12, in C. Tropea, A. Yarin, and J. Foss, Springer Handbook of Experimental Fluid Mechanics, Springer-Verlag Heidelberg, 2007.

[17]M. Drela and M. Giles, “Viscous-Inviscid Analysis of Transonic and Low Reynolds Number Airfoils,” AIAA J., **25**, 1347(1989).

APPENDIX A: THE BOUNDARY LAYER THICKNESS

The following is a short summary of the relevant "unbounded" boundary layer thickness equations from the earlier report.[2] There are two sets of equations, one for the viscous region and a second for the inertial region.

For the viscous region, the equations are similar to those developed originally for the description of the traditional boundary layer.[3,4] However, there is one caveat that was discovered in the earlier NACA0012 report that is relevant to all second derivative based viscous boundary layer descriptions. It was found that the second derivative kernel in the APG region of the NACA0012 airfoil actually had negative values in the near wall region.[2] The moment based boundary layer description is based on the boundary layer kernels behaving like probability density functions. Probability density functions cannot take on negative values. Although the near wall region had negative values, the remaining curve was still Gaussian-like. Therefore, a modified second derivative integral kernel was developed by simply changing the integral limits. This leaves us with a proper probability density function like curve. Hence, we define the viscous velocity boundary layer *n*th central moment, ζ_n for APG based wall-bounded 2-D laminar flow as

$$\zeta_n = -\frac{1}{\alpha}\int_{\omega}^{h} dy\,(y-\omega)^n \frac{d^2u(x,y)}{dy^2} \quad , \tag{A1}$$

where $y=h$ is deep into the free stream, where we take ω as the y-value at the second derivatives negative maximum, and where the normalizing parameter is

$$\alpha = -\int_{\omega}^{h} dy \frac{d^2u(x,y)}{dy^2} \quad . \tag{A2}$$

The viscous boundary layer width, σ_ζ, is defined in terms of the second central moment as $\sigma_\zeta = 2\sqrt{\zeta_2}$. The four-sigma viscous boundary layer thickness δ_v is then defined as $\delta_v = \omega + 4\sigma_\zeta$. The central moments can be used to define shape parameters based on the third and fourth moments in a fashion similar to the method described by Weyburne.[3,4] Although primarily intended for the APG region, the above method should work for the ZPG and FPG regions as well. One of the intentions of the boundary layer moment method is to describe where the viscous forces are no longer significant. Therefore, modifying the integral limits is appropriate as long as the result serves the purpose.

To mathematically define the inertial boundary thickness $\delta_i(x)$ we cast the velocity profile into a probability density function moment framework. To do this we define velocity profiles central moments of $(u(y)/u_\infty)-1$ as

$$\gamma_n \;=\; \int_{\delta_{\max}}^{h} dy\,(y-\kappa)^n\,\frac{1}{\delta_1^i}\left\{\frac{u(y)}{u_\infty}-1\right\} \quad , \tag{A3}$$

where $y = h$ is deep into the free stream, where the mean location κ is given by

$$\kappa \;=\; \int_{\delta_{\max}}^{h} dy\; y\,\frac{1}{\delta_1^i}\left\{\frac{u(y)}{u_\infty}-1\right\} \quad , \tag{A4}$$

and where the modified inertial displacement thickness is

$$\delta_1^i \;=\; \int_{\delta_{\max}}^{h} dy\left\{\frac{u(y)}{u_\infty}-1\right\} \quad . \tag{A5}$$

At this point we can go ahead and construct the various thickness and shape parameters in terms of the mean location and higher order moments of γ_n as was demonstrated by Weyburne.[3] The two-sigma $\delta_{i2}(x) = \kappa + 2\sigma_i$ value where $\sigma_i = \sqrt{\gamma_2}$, for example, corresponds to the point where $u(x, y)$ essentially becomes the free stream velocity u_∞. Although we defined the lower limit in terms of $\delta_{\max}(x)$, it would be equally appropriate to use $\delta_v(x)$ instead depending on the circumstances.

APPENDIX B: POTENTIAL FLOW ESTIMATION OF THE INERIAL BOUNDARY LAYER THICKNESS

The following is a potential flow argument developed by Nigam[8] as a way to set inlet and outlet boundary extents in CFD simulations (it is reproduced almost verbatim with permission). If one assumes the obstacle in Fig. B1 is the viscous boundary layer, then this potential flow argument below basically determines the distance necessary for the velocity profile to return the free stream value, i.e. the inertial boundary layer thickness.

Consider an obstacle *Q* as it encounters a uniform flow with velocity *U* (Fig. B1). The obstacle and its wake displace the streamlines of the free stream, and we may think of the flow at large distances from the obstacle as being the sum of a uniform flow and a source.

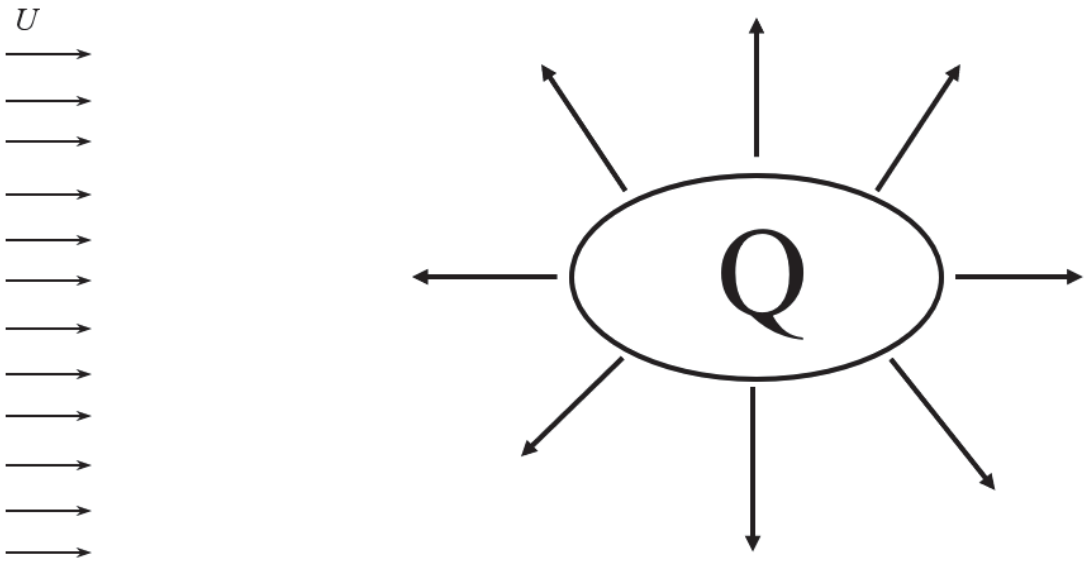

Figure B1: Potential Flow at large distances from an Obstacle and its Wake

The resulting velocity fields in 2-D and 3-D can be expressed as

$$\begin{aligned} (u,v) &= (U+\frac{Qx}{2\pi R^2},\frac{Qy}{2\pi R^2}) \qquad \text{in 2D} \\ (u,v,w) &= (U+\frac{Qx}{4\pi r^3},\frac{Qy}{3\pi r^3},\frac{Qz}{3\pi r^3}) \qquad \text{in 3D} \quad . \end{aligned} \tag{B1}$$

where $R=\sqrt{x^2+y^2}$, $r=\sqrt{x^2+y^2+z^2}$, the source is located at the origin, and the free-stream flow is directed in the positive *x* direction.

The source strength can, in either case, be related to the dimensions of the obstacle. At the *x*-position of the source, the displacement of the streamlines is $y_0=Q/(4U)$ in the 2-D case and $r_0=Q/(2\pi U)$ in the 3-D case. The limiting values far downstream are $y_\infty=Q/(2U)$ and

$r_\infty = Q/(\pi U)$, respectively. For the purpose of the current estimates, either $2y_0$ or $2y_\infty$ in 2-D and $2r_0$ or $2r_\infty$ in 3-D may be used as a representative value for the size of the obstacle. Here, we use $d = Q/(2U)$ in 2-D and $d = \sqrt{2Q/(\pi U)}$ in 3-D. From Bernoulli's equation, we get an estimate of the pressure coefficient at large distances

$$p + \frac{1}{2}\rho|u|^2 = p_\infty + \frac{1}{2}\rho U^2 \quad \Rightarrow \quad C_p = \frac{p - p_\infty}{\frac{1}{2}\rho U^2} = 1 - \left(\frac{|u|}{U}\right)^2 \quad . \tag{B2}$$

Inserting the potential flow velocity fields together with the estimates for the source strengths, we find

$$\begin{aligned} C_p &= -\frac{2}{\pi}\left(\frac{x}{R}\right)\frac{d}{R} + O\left(\left(\frac{d}{R}\right)^2\right) \quad \text{in 2D} \\ C_p &= -\frac{1}{4}\left(\frac{x}{r}\right)\frac{d^2}{r^2} + O\left(\left(\frac{d}{r}\right)^4\right) \quad \text{in 3D} \quad . \end{aligned} \tag{B3}$$

Hence, the pressure coefficient diminishes as d/R in 2D and as $(d/r)^2$ in 3-D. To reduce the influence of the exterior boundary conditions to say $O(10^{-2})$, we would have to locate the exterior boundaries of the computational domain a distance of order of 100 obstacle sizes away in 2-D and 10 obstacle sizes away in 3-D. Applied to boundary layers where the obstacle is the viscous boundary layer, it indicates that the 100 obstacle size distance away would mean the inertial boundary layer thickness would be

$$\delta_i \approx 100\,\delta_v \quad \text{in 2D} \quad , \tag{B4}$$

which is what has been the order of magnitude result observed experimentally in the above unbounded laminar flow result.

APPENDIX C: THE BLASIUS AND FALKNER-SKAN SCALINGS

To test whether or not the Blasius or Falkner-Skan scalings work, it is necessary to scale the simulation results appropriately. In a previous Air Force Tech Report,[15] the Prandtl momentum equations were derived in terms of the displacement thickness $\delta_1(x)$ and velocity at the boundary layer edge $u_e(x)$. Using the stream function approach, the reduced normal velocity for Falkner-Skan flows was show to be

$$\begin{aligned} v(x,y) &= -(m+n)\frac{\delta_1 u_e}{x-x_0} f + n\frac{\delta_1 u_e}{x-x_0}\eta\frac{df}{d\eta} \\ v(x,y)\frac{x-x_0}{\delta_1 u_e} &= -(m+n) f + n\eta\frac{df}{d\eta} \quad , \end{aligned} \tag{C1}$$

where $f(\eta)$ is only a function of η, the *y*-scaling parameter. Since it is assumed that

$$\delta_1(x) = b(x-x_0)^n \quad \text{and} \quad u_e(x) = a(x-x_0)^m \quad , \tag{C2}$$

where x_0, *a*, *b*, *n*, and *m* are constant parameters, then the normal velocity *v*(*x*,*y*) becomes

$$v(x,y)\frac{x-x_0}{\delta_1 u_e} = v(x,y)\frac{x-x_0}{ab(x-x_0)^n(x-x_0)^m} = \frac{1}{ab}v(x,y)(x-x_0)^{(1-m)/2} \quad , \tag{C3}$$

where we have used the fact that similarity requires $m+2n-1=0$. For the $u(x,y)$ profiles, we have

$$\begin{aligned} u(x,y) &= u_e f' \\ \frac{u(x,y)}{a(x-x_0)^m} &= f' \quad . \end{aligned} \tag{C4}$$

The *y*-scaling parameter η for the general Falkner-Skan case goes as

$$\eta = \frac{y}{\delta_1(x)} = \frac{y}{b(x-x_0)^{(1-m)/2}} \quad . \tag{C5}$$

In a similar fashion, the *y*-pressure gradient can be shown to reduce to

$$\frac{(x-x_0)^2}{u_e^2\delta_1}\frac{1}{\rho}\frac{dP}{dy} = -\frac{1}{2}(3m-1)f'' + \frac{1}{2}(1-m)\eta f''' - \frac{1}{4}(m+1)^2 ff' + \\ + \frac{1}{4}(m-1)^2\eta f'^2 - \frac{1}{4}(m+1)(m-1)\eta ff'' \quad , \tag{C6}$$

where we have used the fact that similarity requires that $m+2n-1=0$ and that $b^2 = \nu / a$. Using Eq. C2, the dimensionless *y*-pressure gradient can be shown to reduce to

$$\frac{(x-x_0)^2}{u_e^2\delta_1}\frac{1}{\rho}\frac{dP}{dy} = \frac{1}{\rho}\frac{dP}{dy}\frac{(x-x_0)^2}{a^2 b(x-x_0)^n(x-x_0)^{2m}} = \frac{1}{\rho}\frac{dP}{dy}\frac{(x-x_0)^{(3-5m)/2}}{\sqrt{\nu a^3}} \quad . \tag{C7}$$

For the simulations, herein it was found that setting x_0 to zero is the only value that consistently worked.

LIST OF ABBREVIATIONS, ACRONYMS, AND SYMBOLS

ACRONYM	DESCRIPTION
2-D	Two-Dimensional
3-D	Three-Dimensional
APG	Adverse Pressure Gradient
CFD	Computational Fluid Dynamics
FPG	Favorable Pressure Gradient
RT	Room Temperature
ZPG	Zero-Pressure Gradient